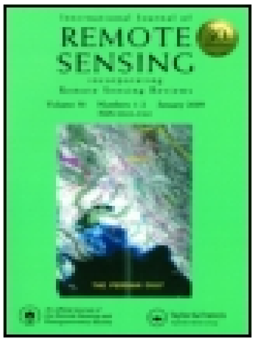

International Journal of Remote Sensing

ISSN: 0143-1161 (Print) 1366-5901 (Online) Journal homepage: https://www.tandfonline.com/loi/tres20

Energy-based cloud detection in multispectral images based on the SVM technique

Yanlin Sui, Bin He & Tianjiao Fu

To cite this article: Yanlin Sui, Bin He & Tianjiao Fu (2019): Energy-based cloud detection in multispectral images based on the SVM technique, International Journal of Remote Sensing, DOI: 10.1080/01431161.2019.1580788

To link to this article: https://doi.org/10.1080/01431161.2019.1580788

Published online: 21 Feb 2019.

INTERNATIONAL JOURNAL OF REMOTE SENSING
https://doi.org/10.1080/01431161.2019.1580788

Energy-based cloud detection in multispectral images based on the SVM technique

Yanlin Sui [a,b], Bin He [b] and Tianjiao Fu [b]

[a]Department of Optoelectronics, University of Chinese Academy of Sciences, Beijing, China; [b]Changchun Institute of Optics, Fine Mechanics and Physics, Chinese Academy of Sciences, Changchun, China

ABSTRACT
In this paper, the energy characteristics of Gabor texture are used for cloud detection in high-resolution multispectral images. First, the satellite remote-sensing image is divided into superpixels using simple linear iterative clustering (SLIC), and then, the energy characteristics of Gabor texture and spectral characteristics are computed by extracting the texture features of the superpixels. The features of the cloud superpixels are used as the learning sample of the support vector machine (SVM) classifier, and a classification model is obtained by training the SVM classifier. Finally, a cloud-detection experiment is conducted for various sensor images with three visible bands and one near-infrared band. The experimental results showed that the proposed method provides an excellent average overall accuracy for thick and thin clouds in a complex background of forests, harbours, snow and mountains. The characteristic parameters of this paper are not limited by the image parameters; thus, they provide good results and universality for various types of sensors.

ARTICLE HISTORY
Received 5 May 2018
Accepted 18 December 2018

1. Introduction

With the rapid development of optical remote-sensing image technology, the number of remote-sensing satellites with high gray level, higher resolution and more spectral bands is increasing. However, cloud occlusions not only cause false interpretation of images but also storage waste due to invalid information. Clouds are unavoidable pollutants of optical images in the visible and infrared spectral ranges, and the generation of a cloud mask associated with remote-sensing images is an important problem. Cloud masks provide both an outlet for images and cloud information. In contrast to popular object detection methods, cloud detection includes a predictive bounding box, and therefore the pixel precision of the mask is important for removing cloud-contaminated pixels during advanced processing.

In recent years, many researchers have studied cloud detection using various types of remote-sensing data. Most researchers use remote-sensing images from multiple spectral segments, such as the eight bands of the Landsat 6, 7 satellite with ETM+ sensors (Zhu and Woodcock 2012) or the Landsat 8 with the newly added shortwave infrared band (1.360–1.390) with OLI sensors (Xu et al. 2016) (Candra, Phinn, and Scarth 2017), for

CONTACT Yanlin Sui yanlinsui@gmail.com University of Chinese Academy of Sciences, Beijing 100049, China

cloud detection. The multitemporal cloud-detection method usually achieves higher cloud-detection accuracy than does the single-image cloud-detection method (Heiselberg and Heiselberg 2017)(Tseng, Tseng, and Chien 2008)(Zhang, Qin, and Qin 2010). However, this method requires more scenes in a short time to ensure that the land cover in a location does not change greatly.

Because of the low demand for input data, the single-image cloud-detection method is more popular than the multi-phase method. Moreover, machine learning has been applied to automatic cloud detection. The parallax feature is highly effective, but its calculation requires parameters such as the orbital height and speed of the panchromatic (PAN) image, which are not always available in image processing (Latry, Panem, and Dejean 2007). (Li et al. 2015) and (Tan, Qi, and Ren 2016) used support vector machines to detect clouds in high-resolution single spectra, whereas (Zhaoxiang et al. 2018) and (Le Goff et al. 2017) used deep learning. However, most current cloud-detection methods use eight bands or images containing a thermal infrared band or a water absorption zone, which are key for cloud recognition. When spectral information is insufficient, cloud detection has limitations. However, many optical satellite imaging sensors have only four bands of spectral information. Thus, studying the use of limited spectral information to detect clouds is of great relevance.

(Li et al. 2017) proposed an automatic multiple feature combination (MFC) method for cloud and cloud shadow detection in GF-1 WFV images. The WFV imaging system is one of the key instruments for GF-1 satellites; it includes four sets with 16-metre spatial resolution, and each WFV camera has four bands spanning the visible near-infrared spectral region. The panchromatic/multispectral imaging system (PMS) is also a key instrument for the GF-1 satellite; it includes two 8-metre spatial resolution systems, four bands of the same WFV and a bandpass similar to that of the Landsat satellite ETM +. However, the parameters in the method presented in the literature only apply to the processing of GF-1 WFV data. Depending on the spectral radiation difference of the sensor itself and the method in (Li et al. 2017), different sets of parameters are needed for multispectral images of different resolutions.

Simple linear iterative clustering (SLIC) was originally proposed by (Zitnick and Kang 2007), and the algorithm has been improved (Kim et al. 2013). In recent years, computer vision applications have become increasingly dependent on superpixels (Achanta et al. 2010)(Hsu and Ding 2013), which have been implemented by parallel GPU acceleration (Ren, Prisacariu, and Reid 2015) and were recently used in the field of remote-sensing images (Csillik 2017) (Zhang et al. 2015). The concept of energy is often used in pattern recognition for gait recognition (Kusakunniran et al. 2009), edge detection (Adelson et al. 1984) and active contour extraction citep(Zhang, Song, and Zhang 2010). The method (Laws 1980) is proposed for classifying each pixel of a texture image to segment the scene. Texture energy has potential for image processing when the intensity distribution is uneven, and the calculation budget is low (Wang et al. 2009) (Zhang, Song, and Zhang 2010).

This paper proposes a cloud-detection method based on Gabor energy, which uses texture energy and the spectral characteristics of four spectral images in combination with SVM to learn training characteristics. This approach can be applied for various sensors and resolutions, yield high precision in snow-covered areas and highlight background areas with limited bands and few features. First, the satellite remote-sensing image is divided into superpixels using SLIC. Then, the energy characteristic of the Gabor texture and the spectral characteristics are computed by extracting the texture features of the superpixel. The features of the cloud superpixels are used as the learning sample for the SVM classifier, and the classification model is obtained by training the SVM classifier. Finally, a cloud-detection experiment is conducted for various sensor images. The experimental results show that the proposed method has an average overall accuracy as high as 92.5% for thick and thin clouds with three visible bands and one near-infrared band in a complex background of forests, harbours, snow and mountains. Good cloud-detection results are achieved for the 16 meter wide-field GF-1 image (level 2A), 8 meter high-resolution GF-1 image (level 1A) and 5.8 meter high-resolution ZY-3 image.

2. Proposed method

2.1. *SLIC*

In general, machine-learning cloud-detection methods take each pixel as a unit, which is time consuming and produces fragmented noise. In this paper, the remote-sensing image is divided into superpixels using SLIC, and the following steps are performed with the superpixel as the basic unit. SLIC uses the K-means algorithm to generate hyperpixels and has the following advantages:

(1) By limiting the search space to areas proportional to the pixel size, the number of distance calculations in the optimization is significantly reduced, which reduces the linear complexity of the pixel N and is independent of the number of pixels K.
(2) The weighted distance measures the combination of colour and space proximity while providing control over the size and compactness of the superpixel.

SLIC methods similar to the pre-processing steps described in (Zitnick and Kang 2007) for depth estimation have not been studied with regard to hyperpixels. SLIC performs a local clustering of pixels and can generate compact superpixels as a subregion that adheres well to regional boundaries. According to (Achanta et al. 2012), the cluster is applied to the CIELAB colour space defined by the L, a, values and the 5-D space of the x and y pixel coordinates. A simple definition of D for the 5-D Euclidean distance in lab xy space will result in inconsistent clustering behaviour under varied pixel sizes. To combine two distances into a single measurement, it is necessary to standardize colour proximity and spatial proximity by their respective maximum distances within the cluster. D' is represented by the following:

$$d_c = \sqrt{(l_j - l_i)^2 + (a_j - a_i)^2 + (b_j - b_i)^2} \tag{1}$$

$$d_s = \sqrt{(x_j - x_i)^2 + (y_j - y_i)^2} \tag{2}$$

$$D' = \sqrt{\left(\frac{d_c}{N_c}\right)^2 + \left(\frac{d_s}{N_s}\right)^2} \tag{3}$$

The maximum spatial distance expected within a given cluster should correspond to the sampling interval, $N_s = S = \sqrt{(N/K)}$. Determining the maximum colour distance N_c is not easy because the colour distance can be significantly different from the cluster and the image; this problem can be simplified by fixing N_c to m

$$D = \sqrt{{d_c}^2 + \left(\frac{d_s}{S}\right)^2 m^2} \tag{4}$$

where m weighs the relative importance of colour similarity and spatial proximity. In the method used in this article, m takes a value of 30.

2.2. *Multispectral information features*

The HOT index (Zhang, Guindon, and Cihlar 2002) has been widely used in smoke abatement and cloud detection (Vermote and Saleous 2007)(Harb, Gamba, and Dell'Acqua 2016). This index is used to separate clouds from clear-sky pixels, considering that the spectral response of the cloud differs from that of most terrestrial surfaces between blue and red wavelengths. The calorific value of cloud pixels is usually greater than that of clear-sky pixels. The mean of the relative HOT ($\overline{H(i)}$) indices in each of the superpixels used in our method can be represented in the following ways:

$$\overline{H(i)} = \sum_i H(i)/N_i \tag{5}$$

and

$$H(i) = \frac{\rho_{(\mathrm{B})_{m_i,n_i}} - 0.5 \cdot \rho_{(\mathrm{R})_{m_i,n_i}}}{\rho_{(\mathrm{B})_{m_i,n_i}} + 0.5 \cdot \rho_{(\mathrm{R})_{m_i,n_i}}} \tag{6}$$

where i and N_i denote the label number of the superpixel and the number of pixels in superpixel i, respectively, and (m_i, n_i) represents the coordinates within superpixel i.

Because the HOT index depends on the band, for high values of the HOT index, the high reflectivity in the visible band and the blue belt of ground objects, such as snow and blue buildings, cannot be excluded from the extracted results, as this causes commission errors in the cloud-detection results. In addition, the ratio of the minimum reflexivity in the visible band to the maximum reflectivity in the visible band can be used to exclude ground objects with other blue, red or green colour features. The mean of the visible band ratio ($\overline{V(i)}$) of the superpixels is as follows:

$$\overline{V(i)} = \sum_i V(i)/N_i \tag{7}$$

where

$$V(i) = \frac{\min\left(\rho_{(\mathrm{B})_{m_i,n_i}}, \rho_{(\mathrm{G})_{m_i,n_i}}, \rho_{(\mathrm{R})_{m_i,n_i}}\right)}{\max\left(\rho_{(\mathrm{B})_{m_i,n_i}}, \rho_{(\mathrm{G})_{m_i,n_i}}, \rho_{(\mathrm{R})_{m_i,n_i}}\right)} \tag{8}$$

V is close to one when the pixel is graygrey. Therefore, VBR can be used to exclude non-cloud pixels with salient colour features from the extracted results.

Because the spectral information of the four spectra is limited, a spectral normalized exponential convergence degree is presented as a feature of the cloud pixel that is trained and identified. Multispectral images (produced by the same camera as the optical remote-sensing images) have different reflection characteristics in different bands, and the reflection of water decreases from the visible wavelength to the infrared wavelength. The near-infrared band has stronger moisture absorption. However, other objects, such as hills, clouds, land and vegetation, do not absorb strongly in near-infrared bands. Normalized indices, such as NDWI, NDSI and NDVI, have been studied using thresholds for preliminary cloud detection (Zhu and Woodcock 2012)(Hagolle et al. 2010)(Manjunath et al. 2015). Thicker clouds are more likely to be treated with a normalized index than other backgrounds because of the high reflectivity in each spectral segment. In this paper, the image hyperpixel subgraph is extracted using the NDWI mean. The NDWI mean in each superpixel is as follows:

$$\overline{\mathrm{NDWI}_i} = \sum_i \mathrm{NDWI}_i / N_i \tag{9}$$

where

$$\mathrm{NDWI}_i = \frac{\rho_{(\mathrm{G})_{m_i,n_i}} - \rho_{(\mathrm{NIR})_{m_i,n_i}}}{\rho_{(\mathrm{G})_{m_i,n_i}} + \rho_{(\mathrm{NIR})_{m_i,n_i}}} \tag{10}$$

$\rho_{(\mathrm{G})_{m_i,n_i}}$ and $\rho_{(\mathrm{NIR})_{m_i,n_i}}$ are the average of the digital number DN value of the green channel and the near-infrared channel in superpixel *i*.

2.3. *Energy characteristics of the Gabor texture*

The spectral characteristics reflect only the relative information between the spectral segments of the local objects and do not fully express scenery features. The spectral characteristics of clouds are shared by snow, glaciers, deserts and other features. Therefore, spectral characteristics cannot distinguish clouds accurately. This paper uses texture features to further describe the characteristics of the cloud. The texture characteristics of the cloud are random. Although the texture element is variable and capricious, it is different from the texture feature of the ground object (Horvath et al. 2002)(Zou and Shi 2016). On the basis of texture feature analysis, a cloud is similar to a ground object to some extent, and the texture features of clouds and ground objects are extracted from the statistical characteristics of the image, which can distinguish the cloud and surface objects effectively. To some extent, part of a cloud is similar to the whole cloud, and the cloud cluster has some fractal similarity. Accordingly, a new cloud-detection method is proposed that can distinguish the energy characteristics of the Gabor texture of clouds and ground objects. Gabor filters are similar in frequency and direction to human visual systems; thus, they are often used for texture recognition ((Zhang et al. 2012). A Gabor transform is a type of windowed Fourier transform, and a Gabor function can extract relevant features under various scales and directions in the frequency domain. In the space domain, a two-dimensional Gabor filter is the product of a Gaussian kernel function and a sine plane; its formula is as follows:

$$g(x,y;\lambda,\theta,\psi,\sigma,\gamma)=\exp\left(-\frac{x'^2+\gamma^2y'^2}{2\sigma^2}\right)\exp\left(i\left(2\pi\frac{x'}{\lambda}+\psi\right)\right) \tag{11}$$

Real

$$g(x,y;\lambda,\theta,\psi,\sigma,\gamma)=\exp\left(-\frac{x'^2+\gamma^2y'^2}{2\sigma^2}\right)\cos\left(2\pi\frac{x'}{\lambda}+\psi\right) \tag{12}$$

Imaginary

$$g(x,y;\lambda,\theta,\psi,\sigma,\gamma)=\exp\left(-\frac{x'^2+\gamma^2y'^2}{2\sigma^2}\right)\sin\left(2\pi\frac{x'}{\lambda}+\psi\right) \tag{13}$$

Where

$$\begin{aligned} x' &= x\cos\theta + y\sin\theta \\ y' &= -x\sin\theta + y\cos\theta \end{aligned} \tag{14}$$

In this equation, λ represents the wavelength of the sinusoidal factor, θ represents the orientation of the normal to the parallel stripes of the Gabor function, ψ is the phase offset, σ is the sigma/standard deviation of the Gaussian envelope, and γ is the spatial aspect ratio, which specifies the elliptical nature of the Gabor function support (Yang et al. 2003).

$(\Delta x,\Delta y)$ represents the direction such that the horizontal distance has Δx pixels and the vertical distance has Δy pixels. The definition of texture energy is used to measure the uniformity of the image greyscale, which can be written as follows:

$$E=\sum_{x,y}(g(\Delta x,\Delta y))^2 \tag{15}$$

2.4. *Algorithm description*

The first SLIC algorithm of an IGB (false-colour composite) image obtains the superpixel sub-picture, extracts the features of the superpixel sub-picture, obtains the classification model of the cloud superpixel sub-picture based on SVM training, and detects the cloud test image. As shown in Figure 1, the classification algorithm is as follows:

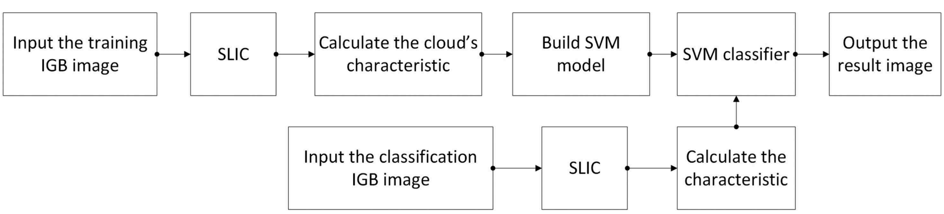

Figure 1. The classification algorithm.

(1) Divide the images into two groups: one for the training set and the other for the test set.
(2) First, SLIC is performed on two sets of IGB (pseudo-colour composite) images to obtain a superpixel segmentation map, and the superpixel cloud in the manually labelled training image is a positive sample.
(3) Extract all the features of the cloud superpixel and the green and near-infrared images of the Gabor texture energy, and train the SVM to obtain the model parameters.
(4) The same method calculates the features of all superpixels in the extracted test image, uploads the SVM classification parameters, and identifies positive classification results as clouds. The algorithm is applied to remote sensing satellite cloud detection. The method training process can be carried out on the ground, the satellites are classified for decision making, and the training parameters are transmitted to the satellite processor through the satellite ground connection.

In this way, the detection ability of satellite cloud images is created, and satellite processing is simplified.

3. Results

To verify the algorithm proposed in the previous section and its superiority and universality, we compare it with the other two methods. As with the first method, the methods in this paper pre-process the image extraction features before implementing the SVM algorithm. The method (Li et al. 2015) is used to determine the sub-blocks of the cloud according to brightness characteristics. In this paper, the superpixel subgraph is obtained by SLIC, and feature extraction is performed by using the superpixel sub-picture as the unit. Another recent study (Li et al. 2017) focused on cloud detection in multispectral high-resolution images – the purpose of which is similar to that in this paper – using only spectra and greyscale from four spectra. The algorithm in (Li et al. 2015) is reimplemented in this paper according to the original description, and the algorithm verification in (Li et al. 2017) is obtained from the images and algorithm programs provided by the author on the website. For comparison, we use the same SVM method as (Li et al. 2015) and obtain the parameters via cross-validation. The images selected herein include GF-1 PMS images, ZY-3 images, and GF-1 WFV images provided in (Li et al. 2017). It is worth noting (Li et al. 2017), as the algorithm program provided by the author only supports image processing of GF-1 WFV. The host computer algorithm in this paper was verified using a hardware environment with a 3.50 GHz Intel(R) Xeon(R) CPU, 64.0 GB RAM and Microsoft Windows 7 Service Pack 1 operating system. The experimental development environment is MATLAB R2014a. The experiment settings are as follows.

3.1. *GF-1 WFV imagery*

The GaoFen-1 (Gao Fen means high resolution in Chinese) satellite was launched by China. Detailed information on GF-1 satellites and WFV images can be found at http://sendimage.whu.edu.cn/en/mfc-validation-data/. The GF-1 WFV image selected herein is a Class 2A product produced by relative radiation correction and system geometry correction. The level-1A data are raw digital products of homogenized radiation calibration, while the level-2A data are produced after systematic geometric correction, in which the pixels are all resampled to a 16 m resolution with 10-bit data. The experimental scene selection includes five types of ports, snow, mountains, forests, and cities to test the cloud-detection performance of the method under various scene types. Images were taken from 2012 to 2017. The images used for training and testing include both thick and thin clouds. For each scene, 100 different oaks are selected for training. The images range in size from 256 × 256 pixels to 1024 × 1024 pixels, and 20 images are selected for testing in each scene. Figure 2 shows four representative original images,

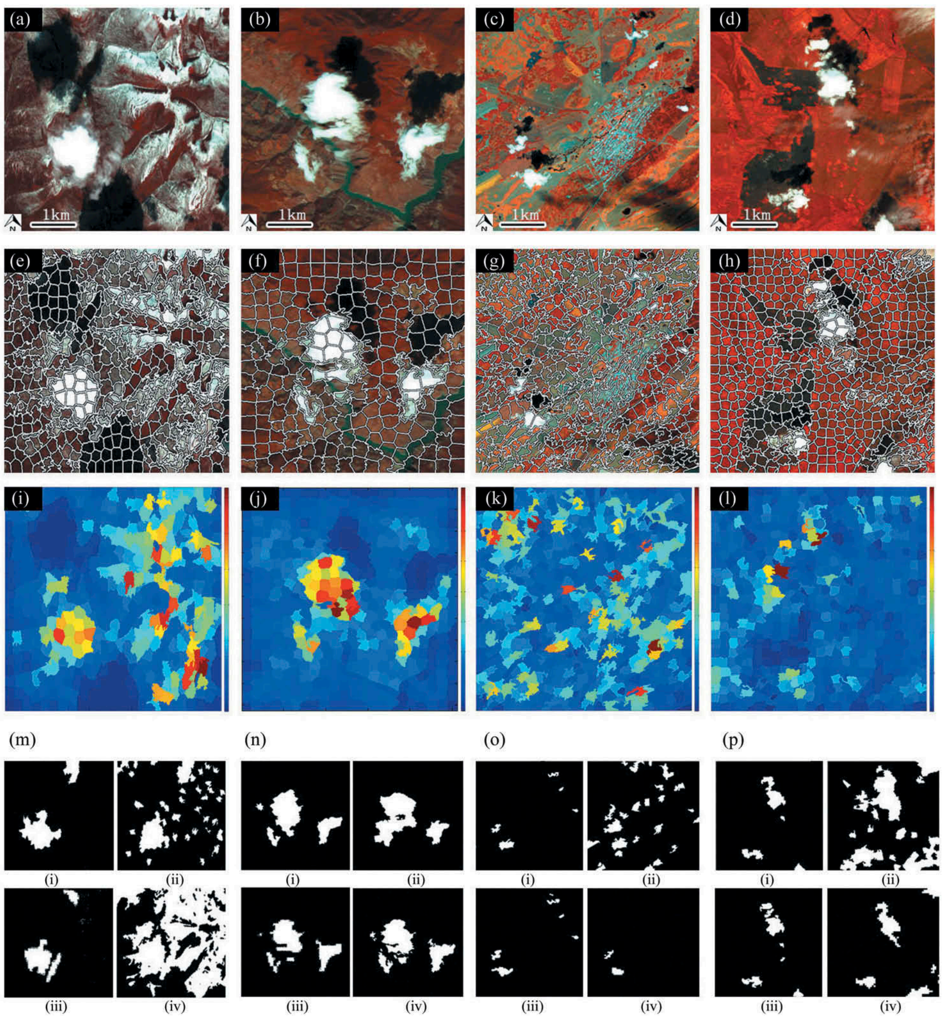

Figure 2. Experiment with GF-1 WFV imagery.(a)GF1 WFV4 E132.4 N53.2 20160507 L2A; (b)GF1 WFV1 E102.0 N28.0 20140302 L2A; (c)GF1 WFV1 E73.7 N56.3 20130712 L2A; (d)GF1 WFV1 E114.9 N23.5 20141008 L2A; (e)Result of SLIC in (a); (f)Result of SLIC in (b); (g)Result of SLIC in (c); (h)Result of SLIC in (d); (i)Result of extracting the Gabor texture energy in (e); (j)Result of extracting the Gabor texture energy in (f); (k)Result of extracting the Gabor texture energy in (g); (l)Result of extracting the Gabor texture energy in (h); (m) (i)Our method,(ii)(Li et al. 2015),(iii)mask and (iv)(Li et al. 2017) results of (a); (n) (i)Our method,(ii)(Li et al. 2015),(iii)mask and (iv)(Li et al. 2017) results of (b); (o) (i) Our method,(ii)(Li et al. 2015),(iii)mask and (iv)(Li et al. 2017) results of (c); (p) (i)Our method,(ii)(Li et al. 2015),(iii)mask and (iv)(Li et al. 2017) results of (d);

the segmentation results of SLIC processing, and the distribution of Gabor energy features. The results were then compared to the methods in (Li et al. 2015) and (Li et al. 2017). The algorithm program of document li(Li et al. 2017) can be downloaded from http://sendimage.whu.edu.cn/en/mfc/, but the program can only be used for cloud detection in MFV images.

3.2. *GF-1 PMS imagery and ZY-3 imagery*

To verify the ubiquity of the methods presented herein, comparative experiments were performed using ZY-3 and GF-1 PMS images. The panchromatic/multispectral (PMS) imaging system is another key instrument operating onboard the GF-1 satellite. This system includes two cameras with an 8-m spatial resolution. The ZiYuan-3 satellite (Zi Yuan means resource in Chinese) has an image resolution of 5.8-m, and the spectral spectrum is the same as that of GF-1 PMS and GF-WFV. Detailed information about ZY-3 satellites and images can be found at http://sjfw.sasmac.cn/en/ZY-3.htm . The selection method of the experimental image is the same as that of the WFV of the GF-1, and Figure 3 shows five representative original images, the segmentation result of SLIC processing, and the distribution of the Gabor energy features. In the process of dividing cloud masks, we first converted the blue, green and near-infrared bands of the original images into 24-bit colour images. Then, we used the Magic Wand tool and Lasso tool in Adobe Photoshop to mark the position of the clouds in the image. Finally, the reference mask was generated by setting the DN values of cloud and non-cloud pixels to 255 and 0, respectively. Figure 3 shows the cloud-detection results for the three remote-sensing images using different methods.

4. Discussion

We compared our method with three other methods, including using the reference mask to evaluate the efficiency of our cloud-detection algorithm. We compared one of Li's cloud-detection methods with the SVM method (Li et al. 2015) and another of Li's cloud-detection methods (Li et al. 2017). Their programs and dates can be downloaded from http://sendimage.whu.edu.cn/en/mfc/, but the program can only be used for the cloud detection of MFV images. In the process of dividing cloud masks, we first converted the blue, green and near-infrared bands of the original images into 24-bit colour images. Then, we used the Magic Wand tool and Lasso tool in Adobe Photoshop to mark the position of the cloud in the image. Finally, the reference mask was generated by setting the DN values of cloud and non-cloud pixels to 255 and 0, respectively. Table 1 shows the cloud-detection results for the three remote-sensing images using different methods.

Furthermore, four metrics were used to quantitatively evaluate the algorithms: right rate (RR), error rate (ER), false alarm rate (FAR), and ratio of RR to ER (RER) (An and Shi 2015).

RR is defined as follows:

$$\mathrm{RR} = \frac{\mathrm{CC}}{\mathrm{GN}} \tag{16}$$

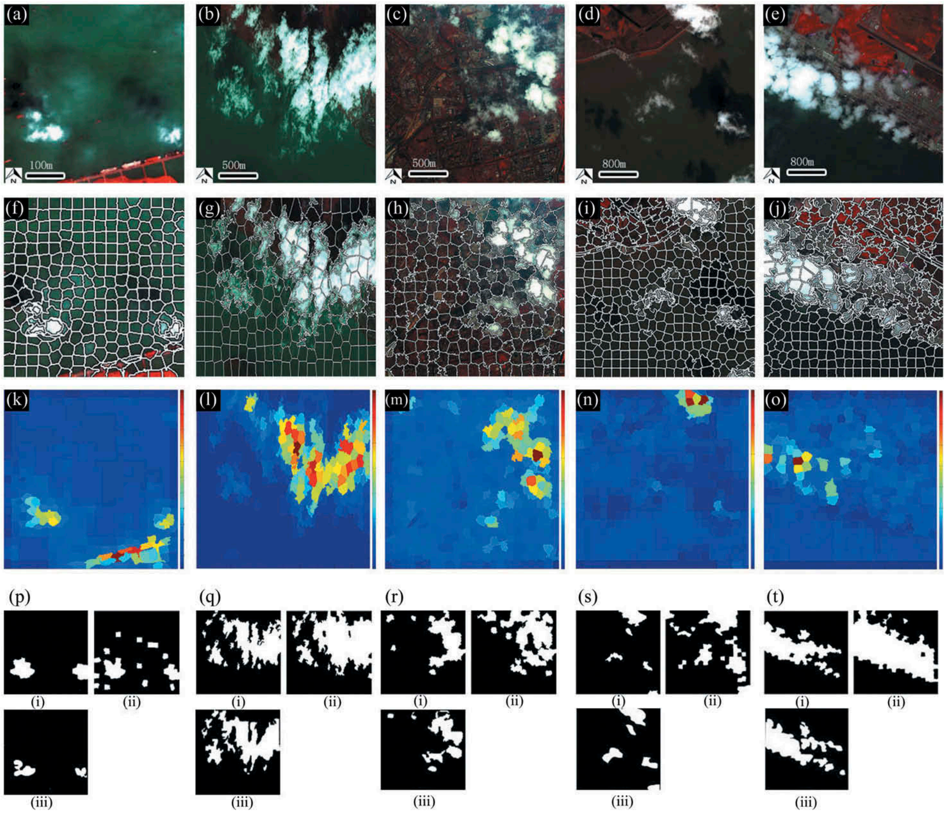

Figure 3. Experiment with GF-1 PMS imagery and ZY-3 imagery.(a)GF1 PMS1 E121.0 N31.920150328 L1A; (b)GF1 PMS2 E121.3 N31.6 20151023 L1A; (c)GF1 PMS1 E113.9 N22.4 20150406 L1A; (d)ZY3 mynfavm 20130606 L1A; (e)ZY3 mux 20150915 L1A; (f)Result of SLIC in (a); (g)Result of SLIC in (b); (h)Result of SLIC in (c); (i)Result of SLIC in (d); (j)Result of SLIC in (e); (k)Result of extracting the Gabor texture energy in (f); (l) Result of extracting the Gabor texture energy in (g); (m)Result of extracting the Gabor texture energy in (h); (n)Result of extracting the Gabor texture energy in (i); (o)Result of extracting the Gabor texture energy in (j); (p) (i)Our method,(ii) (Li et al. 2015) and (iii)mask results of (a); (q) (i)Our method,(ii) (Li et al. 2015) and (iii) mask results of (b); (r) (i)Our method,(ii) (Li et al. 2015) and (iii)mask results of (c); (s) (i)Our method,(ii) (Li et al. 2015) and (iii)mask results of (d); (t) (i)Our method,(ii) (Li et al. 2015) and (iii)mask results of (e);

Table 1. RR, FAR, ER and RER results for the different methods.

	GF-1 WFV imagery				GF-1 PMS imagery				ZY-3 imagery			
Method	RR (%)	FAR (%)	ER (%)	RER (%)	RR (%)	FAR (%)	ER (%)	RER (%)	RR (%)	FAR (%)	ER (%)	RER (%)
Li et al. (2015)	81.77	87.39	36.23	2.26	84.59	55.65	22.13	3.82	82.18	67.56	15.54	5.29
Li et al. (2017)	95.42	96.48	66.91	1.43	-	-	-	-	-	-	-	-
Our method	88.97	26.74	10.82	8.22	91.32	18.64	5.45	16.76	95.38	11.13	7.64	12.48

where CC is the number of pixels correctly detected as a cloud and GN is the number of cloud pixels in the ground truth. ER is defined as follows:

$$ER = \frac{CN + NC}{TN} \tag{17}$$

where CN is the number of cloud pixels detected as non-cloud pixels, NC is the number of non-cloud pixels detected as cloud pixels, and TN is the total number of pixels in the input image. FAR is defined as follows:

$$\mathrm{FAR} = \frac{\mathrm{NC}}{\mathrm{GN}} \tag{18}$$

RER is defined as the ratio of RR to ER:

$$\mathrm{RER} = \frac{\mathrm{RR}}{\mathrm{ER}} \tag{19}$$

As shown in Figures 2 and Figure 3, SLIC is a good way to separate thick clouds from other backgrounds, and extracting features in superpixels can greatly reduce the amount of computation in the process. The Gabor texture energy characteristics proposed in this paper can effectively suppress most backgrounds, such as oceans, houses and forests, and the method accurately identifies the difference between thick clouds and thin clouds. As shown in Table 1 result, this method (Li et al. 2015) has a higher false positive rate because it only considers the luminance characteristics and does not use multispectral features. For the second method of (Li et al. 2017), using the program on its website and comparing it with the method in this paper, the test using the GF-1 MFV database shows that, when a cloud is identified in a snow field, the ER of the method of (Li et al. 2017) is very high; because the texture of the cloud has high energy and combines the information of multispectral spectral segments, the proposed method has a better recognition rate and a lower false positive rate of thick cloud and thin cloud under complex background, and maintains the recognition accuracy. Thus, the proposed method has a wide range of applicability. Because all the parameters required by the method in this paper are not affected by the image parameters, the method in this paper can be applied under various image parameters. All cloud and ground object detection accuracies are high; however, small clouds are not recognized well. Notably, ground object sub-blocks should not be treated as clouds.

5. Conclusions

In general, obtaining satisfactory cloud-detection results for clouds is difficult when images that include visible and near-infrared spectral bands are used. In this paper, a cloud-detection method based on Least squares support vector machines (LS SVM) is proposed that uses SLIC superpixel segmentation to detect thick and thin clouds in four common spectral remote sensing images. The research results of this paper are as follows:

(1) By making full use of the spectral information of four common spectral segments and 10-bit grey-level information, a cloud-detection method based on Gabor texture energy features and spectral features is proposed that compensates for insufficient spectral information for cloud detection in various sensor images.
(2) The method presented in this paper has generality at various resolutions. The model of SVM training, recognition and feature parameters is not affected by sensor parameter differences. Good cloud-detection results are obtained for multispectral images.

(3) The method presented in this paper is promising; it behaves well under most cover conditions, even if the images contain a snow-covered area or a high-illumination background area. The proposed method achieves high precision with limited spectral bands and fewer characteristics.

Acknowledgments

This work was supported in part by the Science and Technology Development Program of Jilin under Grant 20170204029GX. The authors would like to thank Bin He of the Changchun Institute of Optics, Fine Mechanics and Physics, Chinese Academy of Sciences, for his valuable assistance and guidance.

Disclosure statement

No potential conflict of interest was reported by the authors.

Funding

This work was supported by the the Changchun Institute of Optics, Fine Mechanics and Physics, Chinese Academy of Sciences [20170204029GX].

ORCID

Yanlin Sui http://orcid.org/0000-0001-6272-0829

References

Achanta, R., A. Shaji, K. Smith, A. Lucchi, P. Fua, and S. Süsstrunk. 2010. “Slic superpixels.” Technical Report. Lausanne, Switzerland: EPFL Technical Report.

Achanta, R., A. Shaji, K. Smith, A. Lucchi, P. Fua, and S. Süsstrunk. 2012. “SLIC Superpixels Compared to State-Of-The-Art Superpixel Methods.” *IEEE Transactions on Pattern Analysis and Machine Intelligence* 34 (11): 2274–2282. doi:10.1109/TPAMI.2012.120.

Adelson, E. H., C. H. Anderson, J. R. Bergen, P. J. Burt, and J. M. Ogden. 1984. “Pyramid Methods in Image Processing.” *RCA Engineer* 29 (6): 33–41.

An, Z., and Z. Shi. 2015. “Scene Learning for Cloud Detection on Remote-Sensing Images.” *IEEE Journal of Selected Topics in Applied Earth Observations and Remote Sensing* 8 (8): 4206–4222. doi:10.1109/JSTARS.2015.2438015.

Candra, D. S., S. Phinn, and P. Scarth. 2017. “Cloud and Cloud Shadow Removal of Landsat 8 Images Using Multitemporal Cloud Removal Method.” In *Agro-Geoinformatics, 2017 6th International Conference on*, 1–5. Fairfax, VA: IEEE.

Csillik, O. 2017. “Fast Segmentation and Classification of Very High Resolution Remote Sensing Data Using SLIC Superpixels.” *Remote Sensing* 9 (3): 243. doi:10.3390/rs9030243.

Hagolle, O., M. Huc, D. Villa Pascual, and G. Dedieu. 2010. “A Multi-Temporal Method for Cloud Detection, Applied to FORMOSAT-2, VENS, LANDSAT and SENTINEL-2 Images.” *Remote Sensing of Environment* 114 (8): 1747–1755. doi:10.1016/j.rse.2010.03.002.

Harb, M., P. Gamba, and F. Dell'Acqua. 2016. “Automatic Delineation of Clouds and Their Shadows in Landsat and CBERS (HRCC) Data.” *IEEE Journal of Selected Topics in Applied Earth Observations and Remote Sensing* 9 (4): 1532–1542. doi:10.1109/JSTARS.2016.2514274.

Heiselberg, P., and H. Heiselberg. 2017. “Ship-Iceberg Discrimination in Sentinel-2 Multispectral Imagery by Supervised Classification.” *Remote Sensing* 9 (11): 1156. doi:10.3390/rs9111156.

Horvath, G., A. Barta, J. Gal, B. Suhai, and O. Haiman. 2002. “Ground-Based Full-Sky Imaging Polarimetry of Rapidly Changing Skies and Its Use for Polarimetric Cloud Detection.” *Applied Optics* 41 (3): 543–559. doi:10.1364/AO.41.000543.

Hsu, C.-Y., and J.-J. Ding. 2013. “Efficient Image Segmentation Algorithm Using SLIC Superpixels and Boundary-Focused Region Merging.” In *Information, Communications and Signal Processing (ICICS) 2013 9th International Conference on*, 1–5. Tainan, Taiwan: IEEE.

Kim, K.-S., D. Zhang, M.-C. Kang, and S.-J. Ko. 2013. “Improved Simple Linear Iterative Clustering Superpixels.” In *Consumer Electronics (ISCE), 2013 IEEE 17th International Symposium on*, 259–260. Hsinchu, Taiwan: IEEE.

Kusakunniran, W., W. Qiang, L. Hongdong, and J. Zhang. 2009. “Multiple Views Gait Recognition Using View Transformation Model Based on Optimized Gait Energy Image.” In *Computer Vision Workshops (ICCV Workshops), 2009 IEEE 12th International Conference on*, 1058–1064. Kyoto, Japan: IEEE.

Latry, C., C. Panem, and P. Dejean. 2007. “Cloud Detection with SVM Technique.” In *Geoscience and Remote Sensing Symposium, 2007. IGARSS 2007. IEEE International*, 448–451. Barcelona, Spain: IEEE.

Laws, K. I. 1980. “Rapid Texture Identification.” In *Image processing for missile guidance*, Vol. 238, 376–382. San Diego, California: International Society for Optics and Photonics. doi:10.1152/ajpcell.1980.238.5.C169

Le Goff, M., J.-Y. Tourneret, H. Wendt, M. Ortner, and M. Spigai. 2017. “Deep Learning for Cloud Detection.” *8th International Conference of Pattern Recognition Systems,* Madrid, Spain.

Li, P., L. Dong, H. Xiao, and X. Mingliang. 2015. “A Cloud Image Detection Method Based on SVM Vector Machine.” *Neurocomputing* 169: 34–42. doi:10.1016/j.neucom.2014.09.102.

Li, Z., H. Shen, H. Li, G. Xia, P. Gamba, and L. Zhang. 2017. “Multi-Feature Combined Cloud and Cloud Shadow Detection in GaoFen-1 Wide Field of View Imagery.” *Remote Sensing of Environment* 191: 342–358. doi:10.1016/j.rse.2017.01.026.

Manjunath, K. R., R. S. More, N. K. Jain, S. Panigrahy, and J. S. Parihar. 2015. “Mapping of Rice-Cropping Pattern and Cultural Type Using Remote-Sensing and Ancillary Data: A Case Study for South and Southeast Asian Countries.” *International Journal of Remote Sensing* 36 (24): 6008–6030. doi:10.1080/01431161.2015.1110259.

Ren, C. Y., V. A. Prisacariu, and I. D. Reid. 2015. “gSLICr: SLIC Superpixels at over 250hz.” *arXiv preprint arXiv:1509.04232*, 04232: 1509.

Tan, Y., Q. Ji, and F. Ren. 2016. “Real-Time Cloud Detection in High Resolution Images Using Maximum Response Filter and Principle Component Analysis.” In *Geoscience and Remote Sensing Symposium (IGARSS), 2016 IEEE International*, 6537–6540. Beijing, China: IEEE.

Tseng, D.-C., H.-T. Tseng, and C.-L. Chien. 2008. “Automatic Cloud Removal from Multi-Temporal SPOT Images.” *Applied Mathematics and Computation* 205 (2): 584–600. doi:10.1016/j.amc.2008.05.050.

Vermote, E., and N. Saleous. 2007. *LEDAPS Surface Reflectance Product Description*. College Park: University of Maryland.

Wang, L., L. Chunming, Q. Sun, D. Xia, and C.-Y. Kao. 2009. “Active Contours Driven by Local and Global Intensity Fitting Energy with Application to Brain MR Image Segmentation.” *Computerized Medical Imaging and Graphics* 33 (7): 520–531. doi:10.1016/j.compmedimag.2009.04.010.

Xu, M., M. Pickering, A. J. Plaza, and X. Jia. 2016. “Thin Cloud Removal Based on Signal Transmission Principles and Spectral Mixture Analysis.” *IEEE Transactions on Geoscience and Remote Sensing* 54 (3): 1659–1669. doi:10.1109/TGRS.2015.2486780.

Yang, J., L. Liu, T. Jiang, and Y. Fan. 2003. “A Modified Gabor Filter Design Method for Fingerprint Image Enhancement.” *Pattern Recognition Letters* 24 (12): 1805–1817. doi:10.1016/S0167-8655(03)00005-9.

Zhang, K., H. Song, and L. Zhang. 2010. “Active Contours Driven by Local Image Fitting Energy.” *Pattern Recognition* 43 (4): 1199–1206. doi:10.1016/j.patcog.2009.10.010.

Zhang, L., L. Zhang, D. Tao, and X. Huang. 2012. “On Combining Multiple Features for Hyperspectral Remote Sensing Image Classification.” *IEEE Transactions on Geoscience and Remote Sensing* 50 (3): 879–893. doi:10.1109/TGRS.2011.2162339.

Zhang, X., F. Qin, and Y. Qin. 2010. “Study on the Thick Cloud Removal Method Based on Multi-Temporal Remote Sensing Images.” In *Multimedia Technology (ICMT), 2010 International Conference on*, 1–3. Ningbo, China: IEEE.

Zhang, X., S. E. Chew, X. Zhenlin, and N. D. Cahill. 2015. “SLIC Superpixels for Efficient Graph-Based Dimensionality Reduction of Hyperspectral Imagery.” In *Algorithms and Technologies for Multispectral, Hyperspectral, and Ultraspectral Imagery XXI*, Vol. 9472, 947209. Baltimore, Maryland: International Society for Optics and Photonics.

Zhang, Y., B. Guindon, and J. Cihlar. 2002. “An Image Transform to Characterize and Compensate for Spatial Variations in Thin Cloud Contamination of Landsat Images.” *Remote Sensing of Environment* 82 (2–3): 173–187. doi:10.1016/S0034-4257(02)00034-2.

Zhaoxiang, Z., A. Iwasaki, X. Guodong, and S. Jianing. 2018. “Small Satellite Cloud Detection Based On Deep Learning and Image Compression.” Preprints, 2018020103. doi:10.20944/preprints201802.0103.v1.

Zhu, Z., and C. E. Woodcock. 2012. “Object-Based Cloud and Cloud Shadow Detection in Landsat Imagery.” *Remote Sensing of Environment* 118: 83–94. doi:10.1016/j.rse.2011.10.028.

Zitnick, C. L., and S. B. Kang. 2007. “Stereo for Image-Based Rendering Using Image Over-Segmentation.” *International Journal of Computer Vision* 75 (1): 49–65. doi:10.1007/s11263-006-0018-8.

Zou, Z., and Z. Shi. 2016. “Ship Detection in Spaceborne Optical Image with SVD Networks.” *IEEE Transactions on Geoscience and Remote Sensing* 54 (10): 5832–5845. doi:10.1109/TGRS.2016.2572736.